Meteorol Atmos Phys
DOI 10.1007/s00703-012-0224-6

ORIGINAL PAPER

The influence of geometry on recirculation and CO_2 transport over forested hills

Xiyan Xu · Chuixiang Yi

Received: 17 May 2012 / Accepted: 15 October 2012

Abstract Flow distortion over a forested hill is asymmetric, forming a recirculation region on the lee slope that increases the complexity in understanding atmosphere–biosphere interaction. To understand the complexity, we examine the effect of the geometry of forested hills on recirculation formation, structure, and related CO_2 transport by performing numerical simulations over double-forested hills. The ratio (0.8) of hill height (H) to half length (L) is a threshold value of flow patterns in the recirculation region: below 0.8, sporadic reversed flow occurs; at 0.8, one vortex is formed; and above 0.8, a pair of counter-rotating vortices is formed. The depth of recirculation increases with increasing H/L. The contribution of advection to the CO_2 budget is non-negligible and topographic-dependent. Vertical advection is opposite in sign to horizontal advection but cannot exactly offset in magnitude. Height-integrated advection shows significant variation in fluxes across hills. Gentle slopes can cause larger advection error. However, the relative importance of advection to CO_2 budget is slope-independent.

Responsible editor: X.-Y. Huang.

X. Xu · C. Yi (✉)
School of Earth and Environmental Sciences,
Queens College, City University of New York,
65-30 Kissena Blvd, Flushing, NY 11367, USA
e-mail: cyi@qc.cuny.edu

X. Xu · C. Yi
The Graduate Center, City University of New York, New York,
NY 10016, USA

1 Introduction

A large part (70 %) of the earth's land surface is covered with mountains and hills. These rugged surfaces, particularly those covered with forests, distort airflows near the ground and create complexity in understanding land–atmosphere exchanges of mass and energy (Whiteman 2000; Kaimal and Finnigan 1994). One of the most important features in the distorted flows is recirculation formed behind forested mountains or hills (Finnigan and Belcher 2004; Kim et al. 2001; Ross 2008; Poggi and Katul 2007). These recirculation bubbles (regions) operate through different mechanisms to influence mass and energy exchange between forests and atmosphere, such as wind direction alteration and scalar redistribution (Katul et al. 2006; Ross 2011). Because of its importance, studies of recirculation over a forested hill have recently received more attention in experiments, numerical simulations and analytical models. Almeida et al. (1993) found in their water tunnel experiments that the length of recirculation formed behind a single hill is longer than that between multiple hills. Katul's research group at Duke University has investigated the influence of canopy density on recirculation formation by flume experiments (Poggi and Katul 2007). Recirculation formation behind forested hills has been studied by many numerical models (e.g., Dupont et al. 2008; Ross 2008). These numerical simulations have focused on the turbulent characteristic of recirculation. Although Yi (2009) pointed out that a terrain slope is one of the most important control factors to terrain-induced canopy flows, the impact of terrain slopes on recirculation development is still poorly understood.

The goal of this paper is to explore the dependence of recirculation development on terrain geometry using computational fluid dynamics (CFD) method. We employed the renormalization group (RNG) k–ε model developed by

Published online: 31 October 2012

Yakhot and Orszag (1986) to simulate airflows in double-forested hills of different shapes to analyze formation conditions and the structure of recirculation. In order to understand how the scalar transport processes are affected by recirculation development and its complexity, we studied the distribution of advective CO_2 fluxes over forested hills with different hill shapes. The numerical model and design of the simulation are described in Sect. 2. Numerical simulation results and discussions are given in Sect. 3, and concluding remarks in Sect. 4.

2 Method

2.1 Numerical implementation

The computational domain extends over 1,400 × 200 m in a Cartesian grid, corresponding to 700 × 151 grid intervals in the x and y directions. Double hills covered with 15 m tall forest canopy occupy the middle 200 m domain horizontally. The horizontal resolution at forested hills is 1 m and at the bare flat ground is stretched with a power law, starting with a horizontal grid spacing of 1 m at the edge of the forest. The meshes are stretched in the vertical using a power law, starting with a vertical grid spacing of 0.8 at the surface. The stretching powers in horizontal and vertical are 1.15 and 1.1, respectively. Ground surface roughness height is set to be 0.01. Wind velocity at west boundary is set to be a constant, $u = 3$ m s^{-1}. The upstream of the velocity field is fully developed by the bare ground to be logarithmic velocity profile before reaching the double hills. Pressure is fixed at the top boundary and east boundary, where the pressure is close to 0.0 Pa, relative to the external pressure.

In this study, the topography is specified with double sinusoidal hills (Fig. 1) to include both valley and ridges. The shape function of the hill is defined as

$$H(x) = \frac{H}{2}\cos\left(\frac{\pi x}{2L} + \pi\right), \tag{1}$$

where H is the hill height, L is the half length scale, and x is longitudinal distance with $x = 0$ at the left trough of the first hill. Variation of the slope (H/L) is achieved by changing H with a constant $L = 25$ m.

The porous canopy layer is designed to be horizontally homogeneous along the slope and vertically uniform. Leaf area density (a) is specified as mean values from observation (Yi et al. 2005).

The hill surface is assumed to be a source of atmospheric CO_2. The efflux rate is 4 μmol m^{-2} s^{-1}.

2.2 Conservation of mass and momentum

The momentum and mass balance equations in the canopy sub-layer can be written as (Kim and Baik 2004)

$$\frac{\partial \rho}{\partial t} + \frac{\partial(\rho \bar{u}_j)}{\partial x_i} = 0, \tag{2}$$

$$\frac{\partial \bar{u}_i}{\partial t} + \bar{u}_j \frac{\partial \bar{u}_i}{\partial x_j} = -\frac{1}{\rho}\frac{\partial P^*}{\partial x_i} + \nu \frac{\partial^2 \bar{u}_i}{\partial x_i x_j} - \frac{\partial}{\partial x_j}\left(\overline{u_i' u_j'}\right) - F_{\mathrm{D}i}, \tag{3}$$

where $\overline{u_i}$ and $\overline{u_j}$ are the mean velocity components along x_i and x_j directions, respectively, u_i' and u_j' are the fluctuations from their mean values $\overline{u_i}$ and $\overline{u_j}$, ρ is air density, ν is kinematic viscosity of air, P^* is the deviation of pressure from its reference value and $F_{\mathrm{D}i}$ is the drag force exerted by the canopy elements, which is expressed as

$$F_{\mathrm{D}i} = \frac{1}{2} K_{\mathrm{r}} u_i^2, \tag{4}$$

where K_{r} is the resistance coefficient, which is derived from an empirical relationship given by Hoener (1965),

$$K_{\mathrm{r}} = \frac{1}{2}\left[\frac{3}{2\phi} - 1\right]^2 \tag{5}$$

where ϕ is porosity of the canopy layer, which can be obtained from leaf area density (Gross 1993),

$$\phi = \frac{\sqrt{1 + 4a} - 1}{2a}, \tag{6}$$

F_{D} is zero above the canopy. The detailed settings of hill and canopy properties are listed in Table 1.

2.3 Conservation of scalar quantities

The conservation for scalar CO_2 with mean molar mixing ratio (c) is given by

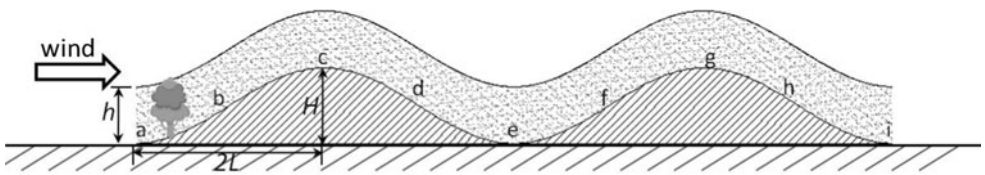

Fig. 1 Schematic diagram of double forested hills. H and L are the height and half-length of hills, respectively. The total length of the double hills is 8L. h denotes the height of canopy. The symbols a–i indicate the locations of nine hypothetical sites across double hills. The horizontal distance between two locations is L

Table 1 Parameters of hill and canopy properties in the model

Parameters	Values
Hill	
L (m)	25
H/L	0.2, 0.4, 0.6, 0.8, 1.0, 1.2, 1.6
Canopy	
h (m)	15
LAI ($m^2\ m^{-2}$)	3.2
a (m^{-1}), Φ	0.22, 0.85

$$\frac{\partial \bar{c}}{\partial t} + \bar{u}_j \frac{\partial \bar{c}}{\partial x_j} = D \frac{\partial^2 \bar{c}}{\partial x_i x_j} - \frac{\partial}{\partial x_j}\left(\overline{c' u_j'}\right) + S_c, \tag{7}$$

where $\overline{u_j}$ is solved by Eqs. (2) and (3), c' is the fluctuation from its mean value $\bar{c}$, D is the molecular diffusivity of CO_2, and S_c is the source of CO_2 from soil respiration.

2.4 RNG k–ε model

The RNG model was developed by Yakhot and Orszag (1986) using the RNG method. RNG k–ε turbulent model has been recognized to be good for separate flows (Speziale and Thangam 1992) and it is superior to the standard k–ε model and Chen's k–ε model (Chen and Kim 1987) when applied to two dimensional valley flows, especially when recirculation is present (Maurizi 2000). Kim and Patel (2000) suggested using the RNG k–ε model to predict the pollutant transport under neutral conditions.

In the RNG k–ε model, the turbulence scheme proposed by Yakhot et al. (1992) is applied. The Reynolds stress in Eq. (3) and turbulent CO_2 flux in Eq. (7) are solved by turbulent viscosity, respectively, as

$$-\overline{u_i' u_j'} = \mu_t \left(\frac{\partial \bar{u}_i}{\partial x_j} + \frac{\partial \bar{u}_j}{\partial x_i}\right) - \frac{2}{3}\delta_{ij} k, \tag{8}$$

$$-\overline{c' u_j'} = \mu_c \frac{\partial \bar{c}}{\partial x_j}, \tag{9}$$

where μ_t and $\mu_c = \mu_t / S_c$ are the turbulent viscosities of momentum and CO_2, respectively, δ_{ij} is Kronecker delta, and k is the turbulent kinetic energy. The turbulent Schmidt number S_c is 0.6 as suggested by Flesch et al. (2002).

It is assumed that turbulence viscosity in Eq. (8) is related to turbulence kinetic energy (k) and dissipation (ε)

$$\mu_t = \rho C_\mu \frac{k^2}{\varepsilon}, \tag{10}$$

where k and ε are determined from the following Eqs. (11) and (12), and C_μ is a dimensionless constant.

The prognostic equation of turbulent kinetic energy and its dissipation are written as

$$\frac{\partial k}{\partial t} + \frac{\partial}{\partial x_j}\left(\bar{u}_j k - \frac{\mu_t}{\sigma_k}\frac{\partial k}{\partial x_j}\right) = P_k + P_w - \varepsilon, \tag{11}$$

$$\frac{\partial \varepsilon}{\partial t} + \frac{\partial}{\partial x_j}\left(\bar{u}_j \varepsilon - \frac{\mu_t}{\sigma_\varepsilon}\frac{\partial \varepsilon}{\partial x_j}\right) = C_{\varepsilon 1}\frac{\varepsilon}{k} P_k - C_{\varepsilon 2}\frac{\varepsilon^2}{k} - S, \tag{12}$$

where P_k is turbulence production given by

$$P_k = \mu \frac{\partial \overline{u_i}}{\partial x_j}\left(\frac{\partial \overline{u_i}}{\partial x_j} + \frac{\partial \overline{u_j}}{\partial x_i}\right) \tag{13}$$

P_w is wake production which is equal to the work done by the flow against form drag (Raupach 1981):

$$P_w = \bar{u}_i F_{Di} = \frac{1}{2} K_r \bar{u}_i^3, \tag{14}$$

S is a volumetric source term given by

$$S = \frac{C_\mu \eta^3 \left(1 - \frac{\eta}{\eta_0}\right)\varepsilon^2}{(1 + \beta_0 \eta^3) k} \tag{15}$$

$$\eta = \frac{k}{\varepsilon}\left[\frac{P_k}{\mu_i}\right]^{1/2} \tag{16}$$

The empirical constants $C_v, \sigma_k, \sigma_\varepsilon, C_{\varepsilon 1}, C_{\varepsilon 2}, \beta_0$ and η_0 are 0.0845, 0.7194, 0.7194, 1.42, 1.68, 0.012, and 4.38, respectively.

3 Results and discussion

3.1 Flow distribution

Figure 2 shows the distributions of streamwise velocity, vertical velocity, and CO_2 concentration in forested hills with different slopes (H/L). It is not surprising that airflow accelerates up the windward slopes and reaches a maximum at crests, and then decelerates on the leeward slopes to the feet of hills, resulting in flow stagnation behind hills, as predicted in many previous studies (Finnigan and Belcher 2004; Belcher et al. 2008). However, our results indicate that the position of the maximum velocity at crests shifts from above canopy into canopy as the slope increases. The shapes of wind profiles on leeward slope and in the valley are substantially different: (1) being logarithmic with gentle slope ($H/L < 0.8$), and (2) exponential as $H/L > 0.8$ (Fig. 3). The transition of the shape of the wind profile behind hills from gentle to steep hill (Fig. 3d, e, h, i) occurs because stagnation becomes stronger and reversed flows appear as slope increases.

The behavior of vertical velocity is more complicated. The most important feature is that the profile of vertical velocity is inflected at the top of the canopy (Fig. 4), i.e., the continuity of vertical velocity gradient ($\partial \bar{w}/\partial z$) is broken at the top of canopy. The vertical velocity gradient

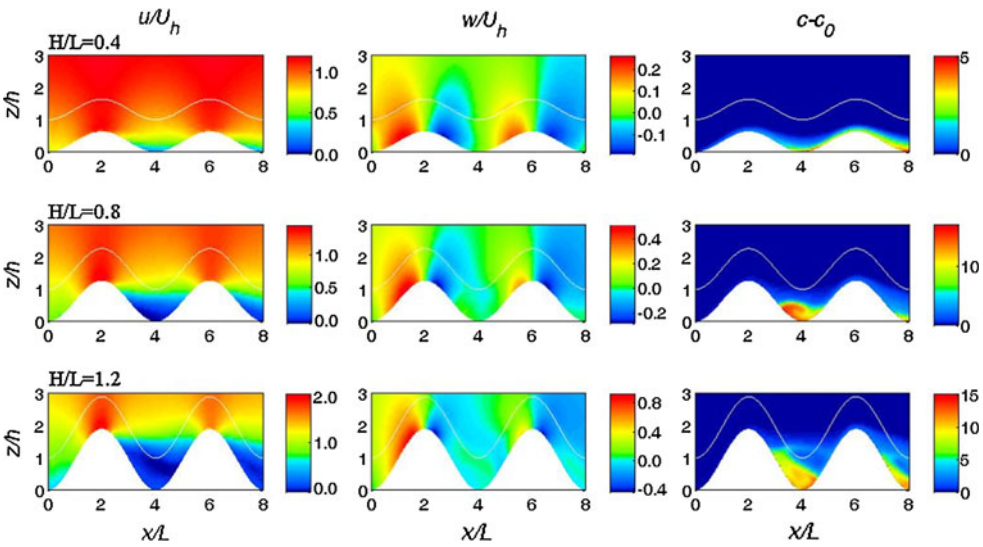

Fig. 2 Mean field distribution of streamwise velocity (u, *left panel*), vertical velocity (w, *middle panel*) and CO_2 mixing ratio ($c - c_0$, *right panel*) for $H/L = 0.4$, 0.8, 1.2. Streamwise velocity and vertical velocity are normalized by the velocity on the top of canopy for each H/L. The CO_2 mixing ratio (in ppm) is represented by the difference from the mean atmospheric CO_2 mixing ratio c_0. *White solid lines* indicate the top of canopy

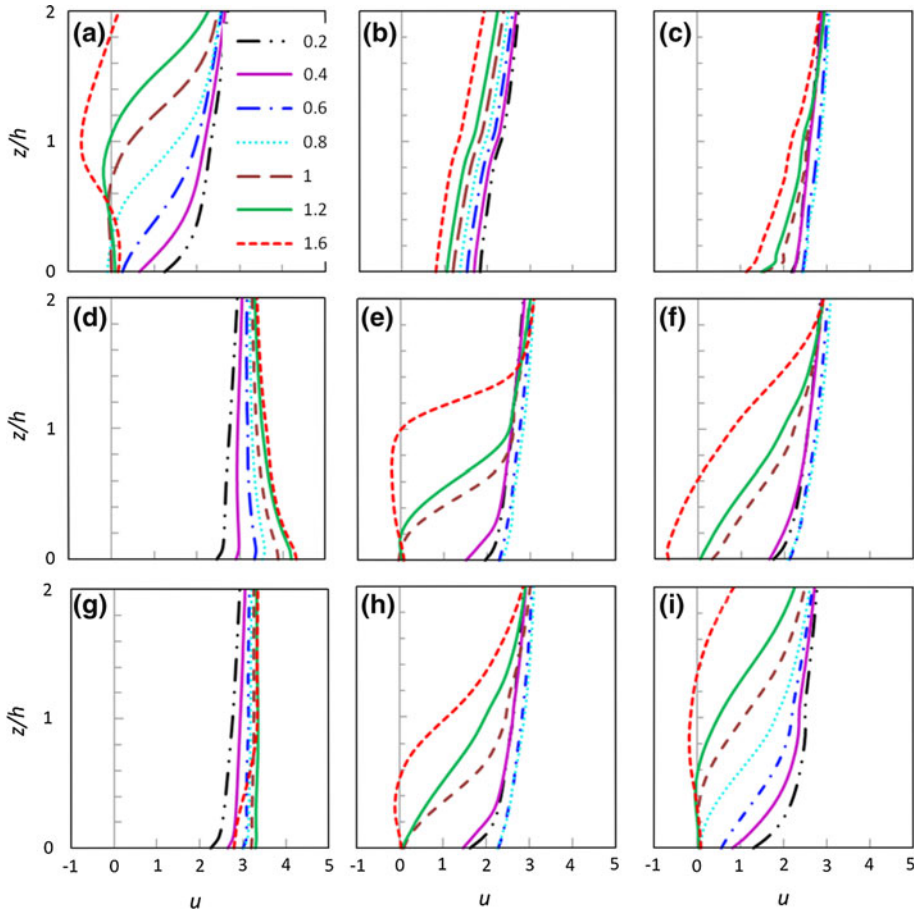

Fig. 3 Profiles of streamwise velocity (u, m s^{-1}) at the hypothetical locations (a–i, shown in Fig. 1) across double hills for $H/L = 0.2$, 0.4, 0.6, 0.8, 1.0, 1.2, and 1.6

is important in calculating vertical advection CO_2 flux. Lee (1998) proposed a method of calculating vertical CO_2 flux by assuming that vertical velocity gradient is constant, in which vertical velocity is assumed to linearly increase from ground to the sensor height of an eddy-flux tower. Lee's method has been widely used in eddy flux communities. However, our simulations indicate that Lee's assumption may be challenged in complex terrain. The vertical velocity is largely inflected at the top of the canopy near forest edges (Fig. 4a, i). The assumption of constant vertical

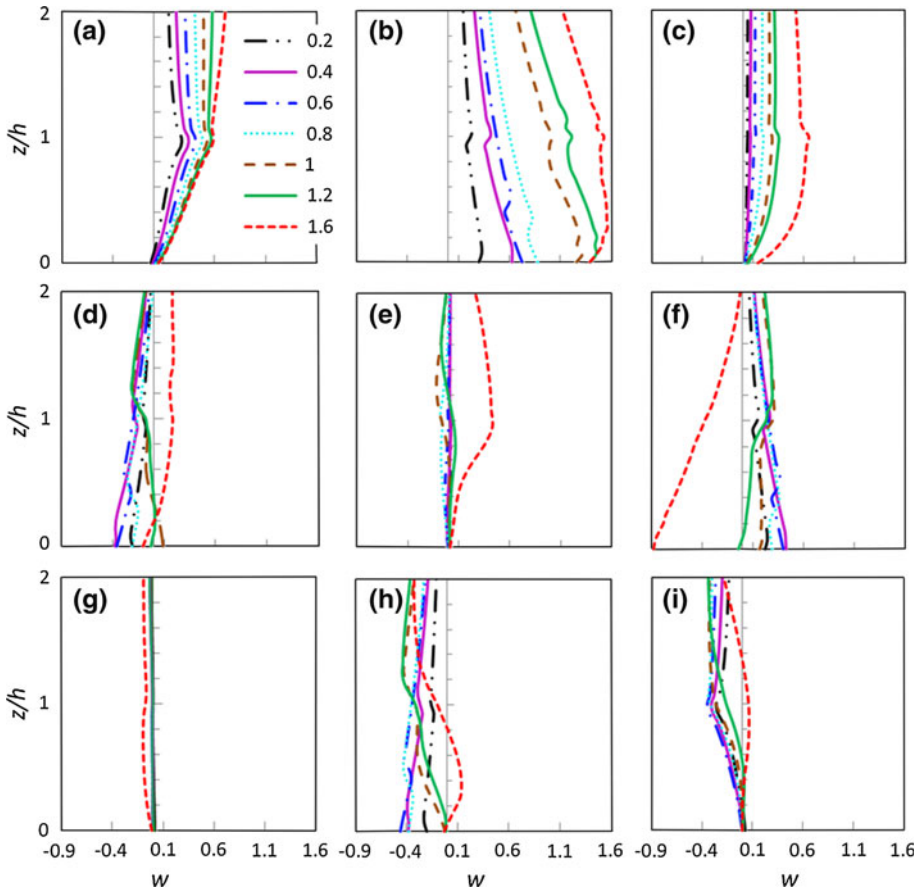

Fig. 4 Profiles of vertical velocity (w, m s^{-1}) at the hypothetical locations (a–i, shown in Fig. 1) across double hills for $H/L = 0.2$, 0.4, 0.6, 0.8, 1.0, 1.2, and 1.6

velocity gradient is valid only for above canopy or within the canopy, but the magnitude and sign of the vertical velocity gradient are different between above and below the top of canopy (Fig. 4a, i). Inflection of vertical velocity around the top of canopy is a common characteristic for all locations across forested hills with low slopes ($H/L \leq 0.4$, Fig. 4). Increasing of slopes enhances vertical velocity significantly. The behavior of the vertical velocity profile becomes complicated on leeward slopes and in the valley (Fig. 4d–f, h) for different slopes, and is closely related to recirculation formation and structure (see discussions in next section).

3.2 Recirculation development

Recirculation is characterized by reversed flow behind hills. It is a region where the flow is decoupled from above mean airflow. Our numerical simulation results indicate that the flow patterns in the recirculation are closely related to hill geometry, which is shown in Fig. 5. $H/L = 0.8$ is a threshold value for flow-pattern formation in recirculation. Our numerical results with gentle hills ($H/L < 0.8$) show that the recirculation is characterized by flows with sporadic negative streamwise velocities at low levels of the canopy layer (Fig. 5a). When H/L is about 0.8, one clockwise vortex is formed in the valley, inclining toward the leeward slope of the hills (Fig. 5b). The inclination of the recirculation vortex behind the second hill is stronger than that of the first hill. The top of a single recirculation vortex can reach the middle canopy layer. When H/L is >0.8, the reversed flow is in the middle to upper canopy layer with a counter-rotating vortex pair (Fig. 5c), which is a common phenomenon on the lee side of mountain barriers (Smolarkiewicz and Rotunno 1989; Bauer et al. 2000; Epifanio 2003). The upper vortex is clockwise and the lower vortex is anti-clockwise. The height of the upper vortex increases with increasing slope and can reach $2.5h$ at $H/L = 1.6$. In comparison with the recirculation formed behind the second hill that extends farther away from the second leeward slope, the recirculation formed in the valley is deeper because flow in the valley is deflected upward by the second hill.

The recirculation formation in the valley or leeward side can be understood by the relative contribution of three major forces within the canopy: adverse pressure gradient (Fig. 6), Reynolds stress gradient, and drag caused by canopy elements. In the upper canopy layer, although adverse pressure gradient and canopy drag act to decelerate mean flow on the leeward slope, the Reynolds stress gradient is large enough to maintain positive streamwise

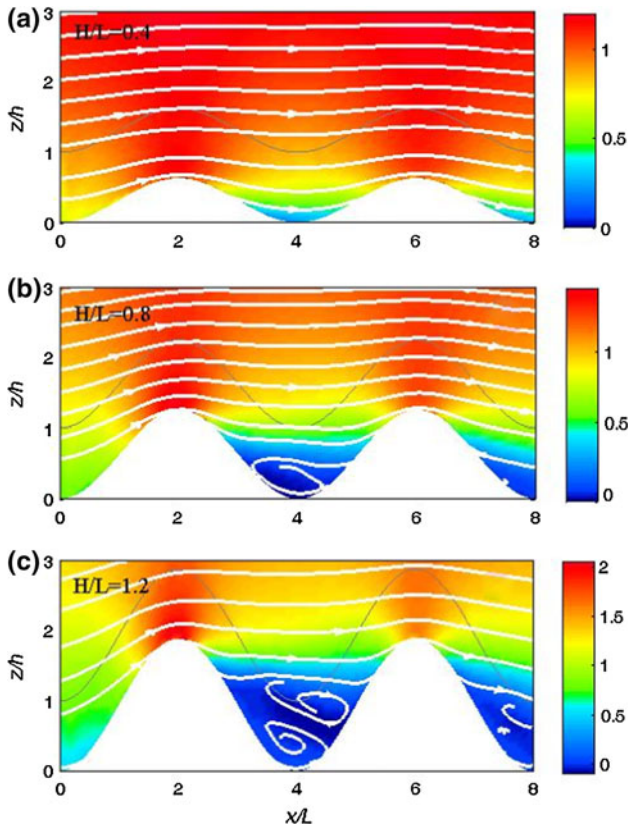

Fig. 5 The streamlines of recirculation patterns for different *H*/*L*: **a** $H/L = 0.4$ (*top panel*), sporadic reversed flow; **b** $H/L = 0.8$ (*middle panel*), one vortex; and **c** $H/L = 1.2$ (*bottom panel*), counter-rotating vortices pair. $H/L = 0.8$ as a threshold value above which two vortices exist, below which no vortex appears, and equal to which only one vortex exists, is valid under condition that the ambient wind satisfies, $1 \leq \bar{u} \leq 5$ (m s^{-1}). The *colored background* indicates mean wind speed (m s^{-1}). *Grey solid lines* indicate the top of canopy. *White solid lines* are streamlines

velocity. In the lower part of the canopy, airflows are dominated by adverse pressure gradient because the observed Reynolds stress profile is exponential (Yi 2008) (Fig. 6) and hence its gradient is very weak. Canopy drag is also weak in the lower part of the canopy because wind speed is low. Thus, reversed flow in the lower part of the canopy (Fig. 5a, b) results mainly from adverse pressure gradient. As slope increases, adverse pressure gradient becomes larger because it is theoretically proportional to the height of hill (Finnigan and Belcher 2004). Consequently, adverse pressure gradient becomes the dominant control even in the upper canopy layer for deep slope hills, which causes the upper vortex formation in upper and just above the canopy layer (Fig. 5c). The lower vortex is a result of dynamic response to the upper vortex.

We define the recirculation depth H_R as the mean height of the flows with streamwise velocity $u = 0$. The depth of recirculation in the valley increases quasi-linearly with slope for both forested and bared hills (Fig. 7a). However, recirculation is deepened by vegetation canopy. The relative contribution of vegetation to the depth of recirculation decreases with *H*/*L* (Fig. 7b). This implies that the effects of canopy layer on recirculation are diminished as slope increases.

3.3 CO_2 transport

3.3.1 CO_2 distribution

The distribution of CO_2 in double-forested hills (Fig. 2, right panel) is primarily dictated by flow patterns of recirculation. When *H*/*L* is smaller than 0.8, ejection from upper canopy occurs behind hillcrests. The ejection has little effect on CO_2 transfer because CO_2 released from slope surfaces is confined to a very shallow surface layer. CO_2 concentration in the recirculation region behind hills could be 4–5 ppm higher than on windward slopes and crests. When *H*/*L* is 0.8, the ejection from the lower canopy behind hillcrests can carry CO_2 to the atmosphere above-canopy in the valley. Large amounts of CO_2 from slope

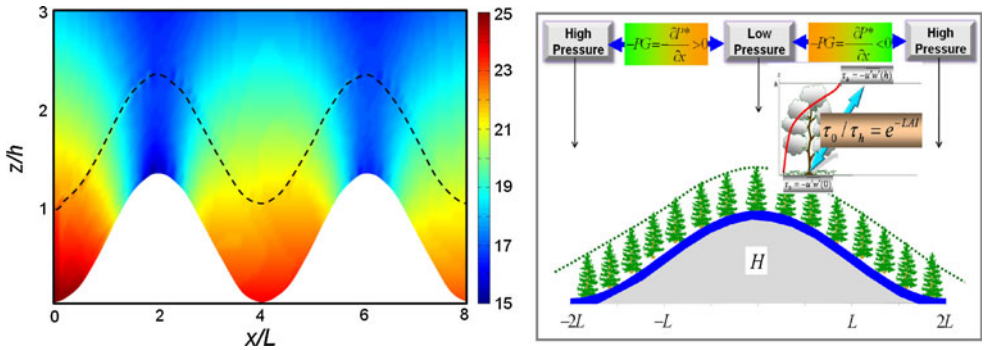

Fig. 6 Deviation of pressure (Pa) from its reference value in the hilly terrain for $H/L = 0.8$ (*left panel*) and a schematic diagram depicting the adverse pressure gradient (−PG) around a single hill which is positive on windward slope and negative on the leeward slope (*right panel*). τ_h and τ_0 are Reynolds stress on the top of canopy and at the ground surface, respectively. The exponential Reynolds stress profile is predicted by a canopy momentum transfer (CMT) model developed by Yi (2008). The *dashed lines* indicate the top of canopy

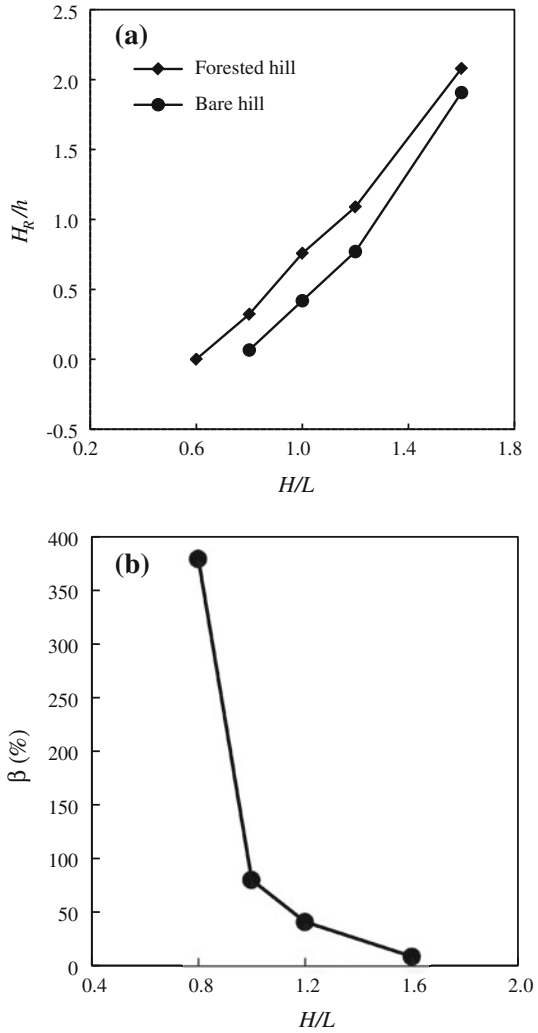

Fig. 7 **a** Depth of recirculation (H_R) in the valley with slope (H/L) for forested hill and bare hill. H_R is the mean height at which level streamwise velocity u is zero in the valley. **b** Relative contribution of canopy to H_R versus slope, H/L. Here, $\beta = \left(H_R^f - H_R^b\right)/H_R^b \times 100\,\%$. H_R^f is the depth of recirculation with canopy and H_R^b the depth of recirculation without canopy

surface circulate in the single recirculation vortex. Because the top of the single vortex is within the middle canopy level, it prevents CO_2 from venting out of the canopy layer, causing as much as a 13 ppm difference in CO_2 concentration between the recirculation vortex on the leeside slope and above-canopy. When H/L is >0.8, CO_2 is partly ejected from the canopy layer to the atmosphere above the canopy in the valley. Transfer of CO_2 into the recirculation region is split into two streams behind hillcrest. One moves downslope, mixing with respired CO_2 from the deep valley, and causing CO_2 to be trapped in the lower recirculation vortex. The other moves downstream then diverts downward upon hitting the windward slope of the second hill, resulting in CO_2 being stored in the upper recirculation vortex. The upper vortex that is located across the top of the canopy is responsible for CO_2 transport from within the canopy to the atmosphere above. Thus, CO_2 concentration in the lower vortex is much higher than in the higher vortex. A double vortex system makes it possible for CO_2 to ventilate from the deep valley to above the canopy, leading to a smaller CO_2 gradient in the canopy layer in comparison with the non-vortex and single vortex recirculation.

3.3.2 *Advective fluxes*

In this study, we explore the CO_2 transfer characteristic in the steady-state neutral atmosphere. Thus, the storage term of CO_2 is not taken into consideration. In steady state, the amount of CO_2 exchange between ecosystem and atmosphere (NEE) is expressed as

$$\mathrm{NEE} = \underbrace{\int_0^{z_r} \frac{\partial\left(\overline{w'c'}\right)}{\partial z}\mathrm{d}z}_{\mathrm{I}} + \underbrace{\int_0^{z_r} \left(\bar{u}\frac{\partial \bar{c}}{\partial x} + \bar{w}\frac{\partial \bar{c}}{\partial z}\right)\mathrm{d}z}_{\mathrm{II}} + \underbrace{\int_0^{z_r} \frac{\partial\left(\overline{u'c'}\right)}{\partial x}\mathrm{d}z}_{\mathrm{III}} \tag{17}$$

where z_r is a reference height above canopy, I is integrated turbulent flux, II is integrated advection fluxes and III is integrated horizontal divergence. The eddy covariance technique (EC) is the most widely used method for quantifying ecosystem carbon flux (Baldocchi 2003). The method was developed to work on perfectly flat topography and homogeneous land-cover. But, it generates significant errors when used to estimate net ecosystem–atmosphere exchange due to neglect of non-turbulent advection fluxes (Eq. 17, II) and horizontal divergence (Eq. 17, III) in complex terrain with heterogeneous vegetation (Aubinet 2008; Sun et al. 2007).

In order to evaluate the influence of recirculation on the CO_2 fluxes, we first evaluate the role of terms I, II and III in NEE. z_r is set to be triple the canopy height ($3h$) and terms I, II and III are averaged along slope to indicate the average contribution of I, II and III to NEE (Table 2). Height-integrated horizontal divergence III is small (III $\ll$ I) in comparison with height-integrated turbulent flux (I) as the slope is gentle ($H/L \leq 0.6$). As recirculation vortices appear ($H/L \geq 0.8$), the ratio of height-integrated horizontal divergence (III) to height-integrated turbulent flux (I) increases. The magnitude of III increases to about 37 % of II as $H/L = 1.6$ due to greater horizontal divergence in the valley. The height-integrated advection flux (II) is comparable with height-integrated turbulent flux (I) in magnitude but opposite in sign. The value of height-integrated advection flux (II) is over 60 % of height-integrated turbulent flux (I) except at $H/L = 1.6$, where it is 30 % of height-integrated turbulent flux (I). The ratio of height-integrated advection

Table 2 The ratio of height-integrated advection flux (II) and horizontal divergence (III) to turbulent flux (I) in Eq. (7)

H/L	II/I	III/I
0.2	−0.82	−0.01
0.4	−1.16	−0.02
0.6	−0.61	0.02
0.8	−0.85	−0.11
1.0	−1.54	−0.36
1.2	−1.00	−0.18
1.6	−0.29	−0.37

flux (II) to height-integrated turbulent flux (I) is independent of slope. The neglect of advection fluxes can cause significant errors in NEE estimations by EC methods in the complex terrain. To further understand the role of advection fluxes in total NEE estimations for different terrain geometry and different positions on the terrain, we use nine hypothetical sites (Fig. 1a–i) to illustrate the spatial variation of advection fluxes across double hills.

Figure 8 shows the distribution of horizontal advective flux $F_h = \bar{u}\partial\bar{c}/\partial x$ (left panel), vertical advective flux $F_v = \bar{w}\partial\bar{c}/\partial z$ (middle panel) and total advective flux $F_T = F_h + F_v$ (right panel) across double hills. Distribution of simulated advective fluxes is strongly dependent on hill geometry. When H/L is <0.8, advective fluxes are important in a very shallow layer within canopy. Horizontal CO_2 flux is positive on the windward slope and negative on the leeward slope. However, the influence of recirculation, which is weak as $H/L < 0.8$, on horizontal advective fluxes is demonstrated by a very shallow layer with positive value in the lower part of the leeside slope. The sign of F_v across the forested hills is mainly determined by the sign of vertical velocity because vertical CO_2 gradient is always negative. The relatively smaller magnitude of advective fluxes observed over the first hill as compared to the second can be explained by the fact that there is better air mixing on the first hill (stronger wind) than the second hill.

When H/L is >0.8, recirculation vortices cause CO_2 to vent out of the deep canopy layer and result in larger advective fluxes scattered and skewed in the valley and in a shallow layer on the slopes. When $H/L = 1.6$, the advective fluxes can become significant even at the level of three-canopy height in the valley. Our simulations demonstrate that F_h and F_v are generally opposite in sign at the same location. However, F_h and F_v cannot exactly offset each other in magnitude as demonstrated in field experiments (Aubinet et al. 2003; Feigenwinter et al. 2008; Yi et al. 2008).

Figure 9 shows the height-integrated advective fluxes at nine hypothetical sites. The sign and magnitude of height-integrated advective fluxes depend on site-locations and slopes. When $H/L < 0.8$, height-integrated F_h and F_v are smaller in troughs (a, e, i) and over crests (c, g), but larger on slopes (b, d, f, h). This is not surprising because the maximum wind velocity over crests can cause better mixing of CO_2, thus very low CO_2 gradient. Although CO_2 gradient is high in the troughs, the stagnated flow leads to small advective fluxes. The location of minimum magnitude of height-integrated total advective flux F_T varies with slopes, which is at h as $H/L = 0.2$, at g as $H/L = 0.4$ and at f as $H/L = 0.6$ (Fig. 9).

Recirculation vortices cause large variations in height-integrated F_h and F_v across double hills when $H/L \geq 0.8$. Although recirculation pattern for $H/L = 1.0$, 1.2 and 1.6 is similar, variation in height-integrated F_h and F_v is significantly different, especially in the valley (d, e, f). When $H/L = 1.2$, the location of minimum magnitude of height-integrated F_T is at h. Even though the individual integrated

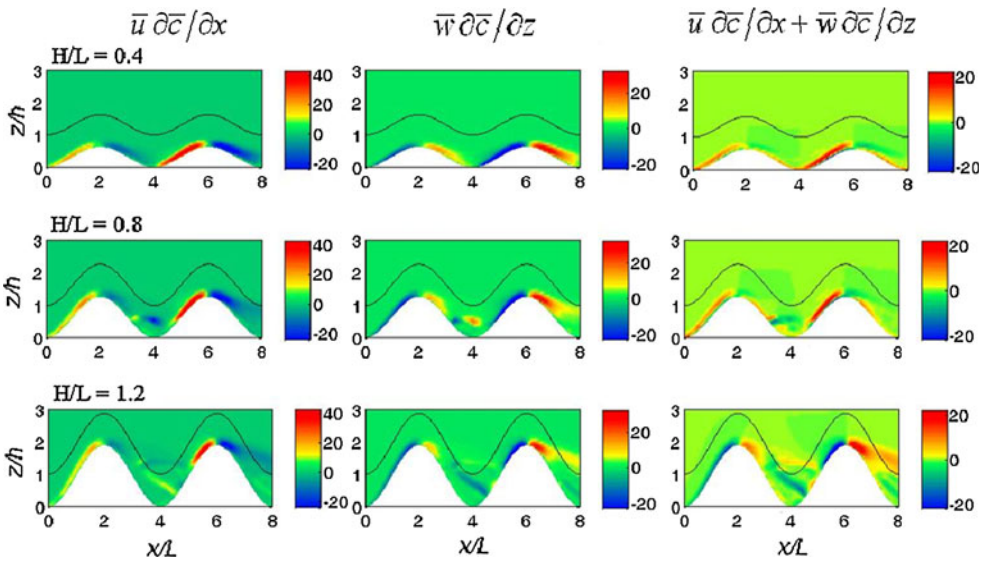

Fig. 8 Spatial variation of advection components (in μmol m^{-3} s^{-1}): horizontal advection ($\bar{u}\partial\bar{c}/\partial x$, *left panel*), vertical advection ($\bar{w}\partial\bar{c}/\partial z$, *middle panel*), and total advection ($\bar{u}\partial\bar{c}/\partial x + \bar{w}\partial\bar{c}/\partial z$, *right panel*) for $H/L = 0.4$, 0.8, 1.2. *Dark solid lines* indicate the top of canopy

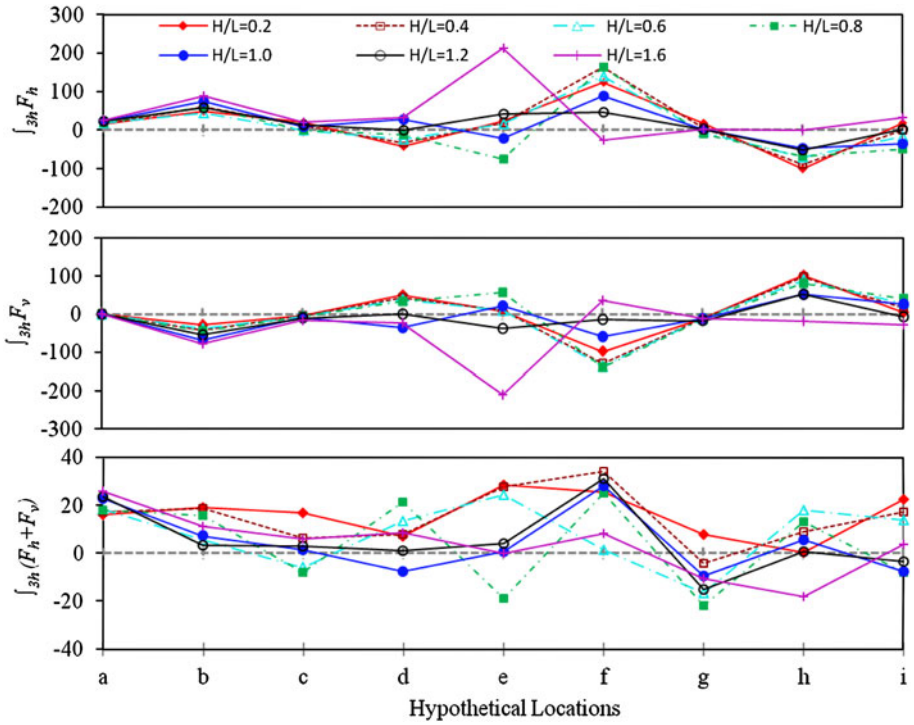

Fig. 9 Height-integrated advective fluxes (in μmol m^{-2} s^{-1}) at hypothetical locations (*a*–*i*, shown in Fig. 1). The advective fluxes are integrated from hill surface to triple the canopy top *h*. $\int_{3h} F_h$, $\int_{3h} F_v$ and $\int_{3h} (F_h + F_v)$ are integration for horizontal advective flux, vertical advective flux and total advective flux, respectively

F_h and F_v are significant in the valley as $H/L = 1.0$ and 1.6, height-integrated F_T are approximate to zero. The different locations of minimum height-integrated F_T indicate that advective error is strongly dependent on hill geometry and flux-tower location in hills.

In order to clarify the overall influence of hill geometry on total advective flux, F_T is integrated through the double-hill domain (Fig. 10). We find that domain-integrated F_T decreases with increasing slope as $H/L \leq 1.0$. Although the relative importance of advective fluxes is slope-independent, the magnitude of advective error could be greater on gentle topographies than steeper ones. We speculate that the decrease of domain-integrated F_T with increasing slope is caused by increasing depth of recirculation that leads to better CO_2 mixing between vegetation and atmosphere.

4 Concluding remarks

The impacts of hill geometry on flow and CO_2 transfer are explored over double-forested hills by numerical approach. We used a double-hill simulation setup, because it can demonstrate flow characteristics not only through hills but also through a valley (i.e., between two hills). Flow recirculation is a typical phenomenon in complex terrain and plays a key role in vegetation–atmosphere exchanges of mass and energy. Our CFD predictions indicate that the complexity and structure of recirculation strongly depend on slope. For gentle forested hills ($H/L < 0.8$), the recirculation structure is simply characterized by reverse flows without vortex, which are limited in the lower part of the canopy layer on leeward sides. The near-surface reverse flows greatly alter CO_2 distribution near the ground rather than enhance CO_2 exchange in vertical. For steep forested hills ($H/L > 0.8$), recirculation bubbles become larger and even deeper than vegetation height with one or multiple vortices, enhancing mixing of CO_2 and energy between vegetation and atmosphere. Consequently, steep slopes cause less advective CO_2 fluxes. The conclusions from numerical experiments provide insights into the issues

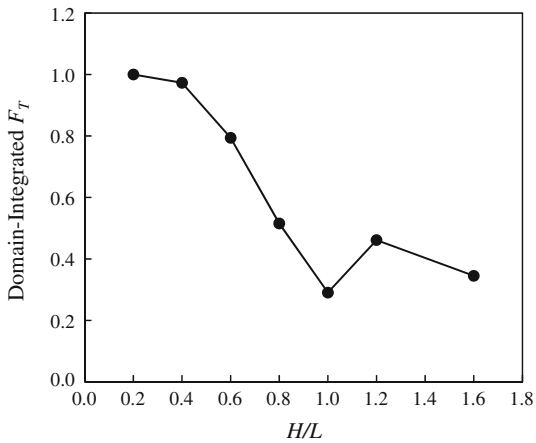

Fig. 10 Domain-integrated total advective flux in double-forested-hill. Total advective flux is integrated in the double-hill domain shown in Fig. 8 to include advective fluxes below and above canopy. The domain-integrated total advective flux is normalized by the domain-integrated total advective flux at $H/L = 0.2$

caused by complex terrain and canopy structure in eddy-flux measurements. However, the flow patterns found under neutral condition in this paper may be different from that under stably stratification. These numerical results also need to be justified by intensive field experiments in the future.

Acknowledgments This research was supported, in part, under National Science Foundation Grants ATM-0930015, CNS-0958379 and CNS-0855217, PSC-CUNY Research Awards (Enhanced) ENHC-42-64, and the City University of New York High Performance Computing Center.

References

Almeida GP, Durao DFG, Heitor MV (1993) Wake flows behind two-dimensional model hills. Exp Therm Fluid Sci 7:87–101

Aubinet M (2008) Eddy covariance CO_2 flux measurements in nocturnal conditions: an analysis of the problem. Ecol Appl 18:1368–1378

Aubinet M, Heinesch B, Yernaux M (2003) Horizontal and vertical CO_2 advection in a sloping forest. Boundary Layer Meteorol 108:397–417

Baldocchi DD (2003) Assessing the eddy covariance technique for evaluating carbon dioxide exchange rates of ecosystems: past, present and future. Glob Change Biol 9:479–492. doi:10.1046/j.1365-2486.2003.00629.x

Bauer MH, Mayr GJ, Vergeiner I, Pichler H (2000) Strongly nonlinear flow over and around a three-dimensional mountain as a function of the horizontal aspect ratio. J Atmos Sci 57:3971–3991

Belcher SE, Finnigan JJ, Harman IN (2008) Flows through forest canopies in complex terrain. Ecol Appl 18:1436–1453

Chen Y, Kim S (1987) Computation of turbulent flows using an extended *k*–epsilon turbulence closure model. NASA CR-179204

Dupont S, Brunet Y, Finnigan J (2008) Large-eddy simulation of turbulent flow over a forested hill: validation and coherent structure identification. Q J Roy Meteorol Soc 134:1911–1929

Epifanio CC (2003) Lee vortices in encyclopedia of the atmospheric sciences. Cambridge University Press, Cambridge, pp 1150–1160

Feigenwinter C, Bernhofer C, Eichelmann U, Heinesch B, Hertel M, Janous D, Kolle O, Lagergren F, Lindroth A, Minerbi S, Moderow U, Mölder M, Montagnani L, Queck R, Rebmann C, Vestin P, Yemaux M, Zeri M, Ziegler W, Aubinet M (2008) Comparison of horizontal and vertical advective CO_2 fluxes at three forest sites. Agric Forest Meteorol 148:12–24

Finnigan JJ, Belcher SE (2004) Flow over a hill covered with a plant canopy. Q J Roy Meteorol Soc 130:1–29

Flesch TK, Prueger JH, Hatfield JL (2002) Turbulent Schmidt number from a tracer experiment. Agric Forest Meteorol 111:299–307

Gross G (1993) Numerical simulation of canopy flows. In: Douglas J, Marcus M (eds) Springer, Berlin, p 167

Hoerner SF (1965) Fluid dynamic drag: practical information on aerodynamic drag and hydrodynamic resistence. Midland Park, NJ

Kaimal JC, Finnigan JJ (1994) Atmospheric boundary layer flows: their structure and measurement. Oxford University Press, New York, p 289

Katul GG, Finnigan JJ, Poggi D, Leuning R, Belcher SE (2006) The influence of hilly terrain on canopy-atmospheric carbon dioxide exchange. Boundary-Layer Meteorol 118:189–216

Kim JJ, Baik JJ (2004) A numerical study of the effects of ambient wind direction on flow and dispersion in urban street canyons using RNG k–ε turbulence model. Atmos Environ 38:3039–3048

Kim HG, Patel VC (2000) Test of turbulence models for wind flow over terrain with separation and recirculation. Boundary Layer Meteorol 94:5–21

Kim JJ, Baik JJ, Chun HY (2001) Two-dimensional numerical modeling of flow and dispersion in the presence of hill and buildings. J Wind Eng Ind Aerodyn 89:947–966

Lee X (1998) On micrometeorological observations of surface–air exchange over tall vegetation. Agric Forest Meteorol 91:39–49

Maurizi A (2000) Numerical simulation of turbulent flows over 2D valleys using three versions of the k–ε closure model. J Wind Eng Ind Aerodyn 85:59–73

Poggi D, Katul GG (2007) Turbulent flows on forested hilly terrain: the recirculation region. Q J Roy Meteorol Soc 133:1027–1039

Raupach MR (1981) Turbulence in and above plant canopies. Ann Rev Fluid Mech 13:97–129

Ross AN (2008) Large-eddy simulation of flow over forested ridges. Boundary Layer Meteorol 128:59–76

Ross AN (2011) Scalar transport over forested hills. Boundary Layer Meteorol 141:179–199

Smolarkiewicz PK, Rotunno R (1989) Low Froude number past 3-dimensional obstacles. Part I: baroclinically-generated lee vortices. J Atmos Sci 46:1154–1164

Speziale CG, Thangam S (1992) Analysis of an RNG based turbulence model for separated flows. Int J Eng Sci 30:1379–1388

Sun J, Burns SP, Delany AC, Oncley SP, Turnipseed AA, Stephens BB, Lenschow DH, LeMone MA, Monson RK, Anderson DE (2007) CO_2 transport over complex terrain. Agric Forest Meteorol 145:1–21

Whiteman CD (2000) Mountain meteorology: fundamentals and application. Oxford University Press, New York, p 355

Yakhot V, Orszag SA (1986) Renormalization group analysis of turbulence: basic theory. J Sci Comput 1:3–61

Yakhot V, Orszag SA, Thangam S, Gatski TB, Speziale CG (1992) Development of turbulence models for shear flows by a double expansion technique. Phys Fluids A4:1510–1520

Yi C (2008) Momentum transfer within canopies. J Appl Meteorol Climatol 47:262–275

Yi C (2009) Instability of analysis of terrain-induced canopy flows. J Atmos Sci 66:2134–2142

Yi C, Monsoon RK, Zhai Z, Anderson DE, Lamb B, Allwine G, Turnipseed AA, Burns SP (2005) Modeling and measuring the nocturnal drainage flow in a high-elevation, subalpine forest with complex terrain. J Geophys Res 110:D22303. doi:10.1029/2005JD006282

Yi C, Anderson DE, Turnipseed AA, Burns SP, Aparks JP, Stannard DI, Monson RK (2008) The contribution of advective fluxes to net ecosystem exchange in a high-elevation, subalpine forest. Ecol Appl 18:1379–1390